*Article*

# Tribological Improvement of Low-Viscosity Nanolubricants: MoO$_3$, MoS$_2$, WS$_2$ and WC Nanoparticles as Additives

José M. Liñeira del Río [1,2,*], Carlos M. C. G. Fernandes [2,3] and Jorge H. O. Seabra [3]

1 Laboratory of Thermophysical and Tribological Properties, Nafomat Group, Department of Applied Physics, Faculty of Physics, and Institute of Materials (iMATUS), Universidade de Santiago de Compostela, 15782 Santiago de Compostela, Spain
2 INEGI, Universidade do Porto, Campus FEUP, Rua Dr. Roberto Frias 400, 4200-465 Porto, Portugal; cfernandes@fe.up.pt
3 Faculdade de Engenharia, Universidade do Porto, Rua Dr. Roberto Frias s/n, 4200-465 Porto, Portugal; jseabra@inegi.up.pt
* Correspondence: josemanuel.lineira@usc.es

**Abstract:** The aim of this research is studying the tribological performance of MoO$_3$, MoS$_2$, WS$_2$ and WC nanoparticles as additives of PAO4. Pure sliding tribological tests were performed at 120 °C, finding outstanding friction and wear reductions in comparison with the PAO4, with maximum friction reductions of 64% for the 0.1 wt% MoS$_2$ nanolubricant and greatest wear decreases for 0.1 wt% MoS$_2$ nanolubricant: a width reduction of 62% and a worn area decrease of 97%. Raman mapping and a roughness evaluation of the worn pins confirmed the tribofilm formation and mending as tribological mechanisms. Rolling–sliding tests were conducted with best nanolubricants performance in pure sliding, observing excellent antifriction capabilities of MoS$_2$ nanoparticles at low speeds, indicating that the use of nanoparticles is vital in boundary lubrication.

**Keywords:** lubricant additives; surface analysis; nanoparticles; rolling–sliding

## 1. Introduction

The growing appearance of electric vehicles (EVs) over the world has led to a great need to develop a large amount of technology that results in obtaining a good consistency and performance of its systems and elements. Specifically, EV manufacturers are demanding new lubricants that possess specific characteristics in order to attain optimal operation in aggressive conditions. Among these necessities, compared to traditional lubricants it can be highlighted elevated thermal conductivity and specific lubricant viscosity (low viscosity), because low-viscosity lubricants lead to important energy savings by decreasing viscous shear and pumping losses [1]. Hence, Gupta [2] valued the efficiency properties of a Toyota Prius changed to operate as an EV utilizing some transmission lubricants that have diverse viscosities, highlighting that an optimum vehicle efficiency increase of about 15% is obtained by utilizing the transmission oil with the lowest viscosity (ATF Lubrizol, 45 cSt@40 °C). Currently, lubricants with optimal performance are composed of base oils of the synthetic type as they possess low viscosities, decent thermal stability and appropriate lubricity. Therefore, it can be stated that this kind of oil can be contemplated as one of the suitable options for the design and enhancement of lubricant oils in EVs. Specifically, polyalphaolefins (PAOs) are the base oils that are most employed because they have optimal tribological properties at high temperatures [3]. However, these base oils require additives to further improve their different properties. Given this fact, nanoparticles (NPs) are, at present, used as base oil additives with remarkable behavior, acting as antiwear and antifriction additives in several research studies [4–7]. Several reasons exist for using NPs as lubricant additives, one of the most significant being their tiny size that allows NPs to be inserted in the contact area, causing a positive lubrication impact [8]. Although there are

numerous articles on NPs as additives of traditional lubricating oils, there are not many articles on NPs with low viscosity oils, so it is important to do more research in this field. In this vein, Mustafa et al. [5] reviewed some experimental works of nanolubricants that exhibit low viscosity, specially PAOs with low viscosity, attaining remarkable results in both friction and wear. These authors found that the greatest tribological behavior was achieved by Kalin et al. [9] with $MoS_2$ nanoparticles as additives of PAO6, lowering the coefficient of friction by two times and the wear more than four times.

In our work, polyalphaolefin 4 (PAO4) was chosen, owing to its low viscosity and for their suitable lubricant properties [10]. Concerning the nanoadditives, $MoO_3$, $MoS_2$, WC and $WS_2$ NPs were utilized as PAO4 base oil additives. $MoS_2$ and $WS_2$ NPs are broadly utilized as additives of lubricants, mainly in conventional base oils, with research on low-viscosity additives, obtaining very good tribological results both in terms of friction and wear, being very scarce [11–18]. For instance, Yu et al. [14] analyzed the tribological behavior of castor oil using $MoS_2$ NPs as additives, reporting that these NPs could decrease the probability of asperities direct contact, causing the decrease in the friction coefficient and also adhesive wear. Furthermore, Nagarajan et al. [11] studied the addition of $MoS_2$ NPs to an SAE 20W50 diesel engine oil, observing that with 0.01 wt% $MoS_2$ concentration, the friction and wear scar diameter were decreased by around 20% for both properties. Additionally, Srivastaba et al. [18] analyzed the tribological performance of the addition of $MoS_2$ and $WS_2$ NPs to castor oil, seeing that the friction was reduced by 50% and 42%, respectively, and the wear scar diameter by 24% and 20%, respectively, compared to castor oil. Furthermore, Ouyang et al. [15] examined the antifriction and antiwear performance of $WS_2$ NPs as castor oil additives, finding that the friction and volume of wear decreased by around 30% and 50%. Concerning the other additives used in this work, $MoO_3$ and WC, there are hardly any works in the literature on their potential use as oil-based lubricant additives. In particular, Sephernia et al. [19] studied the tribological behavior of $MoO_3$-GO-MWCNTs/5W30 hybrid nanolubricants, finding that these nanoadditives reduced the friction coefficient by 6%. Therefore, the authors believe that it is very interesting to research the four different aforementioned nanoadditives with the aim of developing optimized nanolubricants interesting to the industry of EVs. Thus, in the present research, the tribological characteristics of nanolubricants composed of a low-viscosity PAO4 base oil and $MoO_3$, $MoS_2$, WC and $WS_2$ NPs were examined under pure sliding and rolling–sliding settings to find optimal and developed low-viscosity nanolubricants.

## 2. Materials and Methods

The different steps of the experimental studies performed in this investigation are shown in Figure 1 with the aim of better visualizing the different analysis and characterizations to achieve potential low-viscosity nanolubricants.
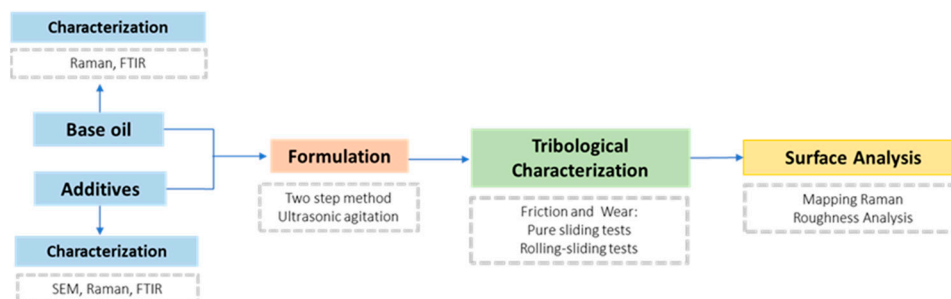


**Figure 1.** Scheme of the methodology performed in this investigation.

### 2.1. Base Oil and Additives

Polyalphaolefin 4 (PAO4) was provided by REPSOL. This oil has a density and dynamic viscosity of 0.8033 g·cm$^{-3}$ and 14.25 mPa·s, respectively, for a T = 313.15 K and a 124-viscosity index. An aliquot of PAO4 was characterized using infrared spectroscopy

(FTIR) and Raman spectroscopy. Thus, Figure 2a reveals the FTIR spectrum: low-intensity peak around 770 $cm^{-1}$ related to alkyl C-C chains, another peak around 1510 $cm^{-1}$ associated with the bending C-H, two strong peaks over 2850–2920 $cm^{-1}$ consistent with the stretching C-H [20]. Furthermore, the Raman spectrum of PAO4 can be seen in Figure 2b. An intense Raman band is found between 2800 and 3000 $cm^{-1}$ with peaks associated to C-H stretching [21] and other peaks around 1310 $cm^{-1}$ and 1440 $cm^{-1}$ related to $\delta(CH_2)$ and $\delta(CH_3)$ vibrations, respectively [22]. Further peaks at 890 and 1080 $cm^{-1}$ can be ascribed to $\nu$(C-C) aliphatic chain vibrations [22].



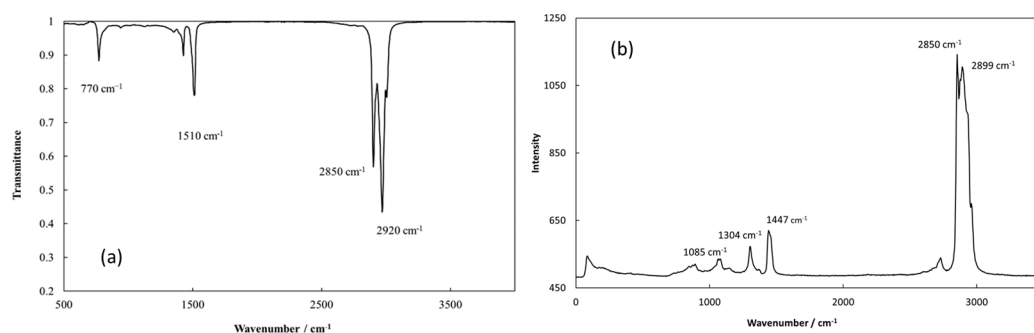**Figure 2.** FTIR spectrum (**a**) and Raman spectrum (**b**) of PAO4 base oil.

Regarding the nanoadditives, four different commercial nanoparticles (US Research Nanomaterials, Houston, TX, USA) were utilized as additives for the PAO4 base oil. Molybdenum oxide nanopowder ($MoO_3$, 1313-27-5) had 99.9% purity, with a size between 13 and 80 nm and with an orthorhombic structure. Molybdenum disulfide nanoparticles ($MoS_2$, CAS number: 1317-33-5) had 99.9% purity, with sizes around 100 nm, a spherical–flaky shape and density of 4.8 $g/cm^3$. Tungsten disulfide nanopowder ($WS_2$, CAS number: 12138-09-9) had 99.9% purity, with a size between 40 and 80 nm, an amorphous structure, flaky shape (thickness 20–50 nm, diameter 50–200 nm) and density of 7.5 $g/cm^3$. Tungsten carbide nanopowder (WC, 12070-12-1) had 99.9% purity, a grain size of 55 nm, a hexagonal shape and density of 15.63 $g/cm^3$. Additionally, according to the information provided by the supplier, the four nanopowders were characterized through different techniques. In the first term, scanning electron microscopy (SEM) was employed to study the morphology of the nanopowders. Figure 3 shows the images of the studied nanoparticles' shape, revealing that the $MoO_3$ nanoparticles have a rectangular shape, which is consistent with having an orthorhombic crystal structure. Regarding the $MoS_2$ nanopowders, it is confirmed that they present a spherical–flaky shape, whereas the $WS_2$ nanoparticles clearly present a hexagonal–laminar shape. Finally, in Figure 3, it is also observed that WC nanoparticles present a hexagonal shape.

Furthermore, all the nanoparticles have been characterized through infrared spectroscopy (FTIR) in order to see the typical bonds related to each nanoparticle. Thus, Figure 4 shows the infrared spectra of the following nanoparticles: $MoO_3$, $MoS_2$, $WS_2$ and WC. The FTIR spectrum of $MoO_3$ nanopowders reveals peaks around 1000 $cm^{-1}$ correlated with the Mo=O asymmetric stretching modes of the extreme oxygen [23,24]. Likewise, peaks at 800 $cm^{-1}$ are linked with the linked oxygen bridge $Mo_2$–O stretching modes [2] of doubly coordinated oxygen. Moreover, bands at 660 $cm^{-1}$ are associated with the triply coordinated oxygen bridge $Mo_3$–O stretching modes [24]. Regarding the FTIR spectrum of $MoS_2$ nanopowders, there are two peaks aligned at 3400 $cm^{-1}$ and at 1630 $cm^{-1}$ that can be attributed to the O-H stretch and modes of bending of $H_2O$, correspondingly [25]. Moreover, peaks at 1135 $cm^{-1}$ and 1065 $cm^{-1}$ are related to the S-O asymmetric stretching, and the peaks around 600 $cm^{-1}$ are consistent with the S-S disulfides stretching [26]. Finally, the existence of the peaks around 900 $cm^{-1}$ and 800 $cm^{-1}$ are correlated with the bending mode of O-H out of plane [27]. Concerning the WC spectrum, it shows an intense group of peaks around 1000 $cm^{-1}$. The one placed around 1150 $cm^{-1}$ is assigned to a WC stretching vibrational mode [28]. Finally, in the FTIR spectrum of $WS_2$ nanopowders, the vibrational

band at 3450 cm$^{-1}$ can be associated with OH of atmosphere and 2900 cm$^{-1}$ band attributed to the vibration bending of W-S [29]. Furthermore, the band that appears at 1640 cm$^{-1}$ can be associated with the vibration of O-H groups [30]. Likewise, the peak located at 1100 cm$^{-1}$ and 600 cm$^{-1}$ appears due to S-S and W-S bonds, correspondingly [30].
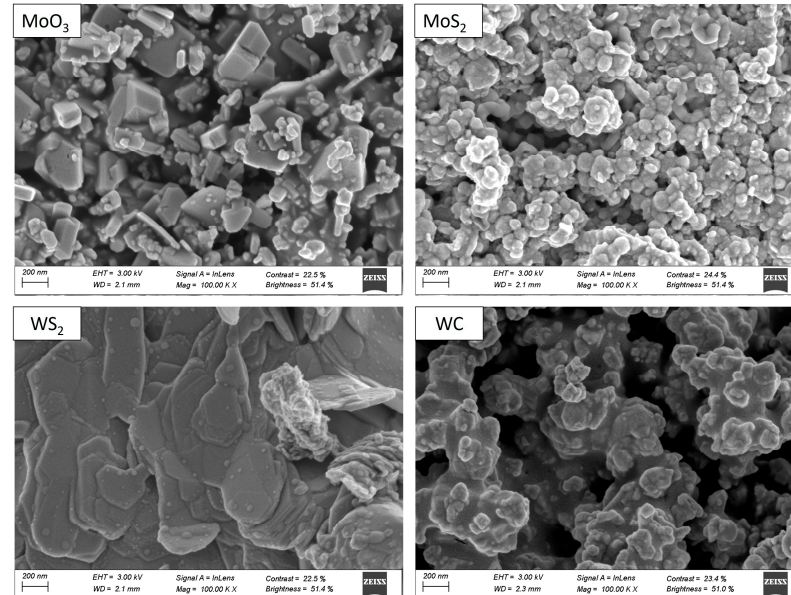


**Figure 3.** SEM characterization of MoO$_3$, MoS$_2$, WS$_2$ and WC nanopowders.
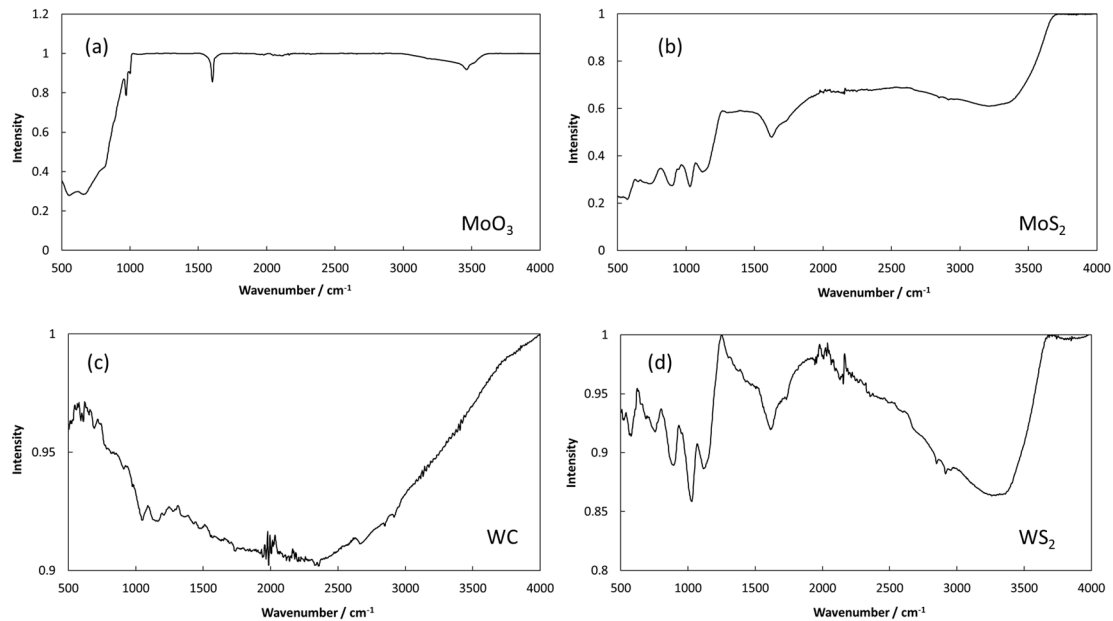


**Figure 4.** FTIR spectra of MoO$_3$ (**a**), MoS$_2$ (**b**), WC (**c**) and WS$_2$ (**d**) nanopowders.

Figure 5 displays the Raman spectra of the following nanoparticles: MoO$_3$, MoS$_2$, WS$_2$ and WC. The Raman spectrum of MoO$_3$ nanopowders reveals peaks around 950 cm$^{-1}$ and 880 cm$^{-1}$ correlated to the asymmetric ($\nu_{as}$ Mo=O$_{(1)}$) and symmetric stretching ($\nu_{as}$ Mo–O$_{(3)}$–Mo) [10,31]. Furthermore, peaks around 700 cm$^{-1}$ and 540 cm$^{-1}$ could be due to asymmetric stretching ($\nu$Mo–O$_{(2)}$–Mo) and the bending mode, in that order [10,31]. Peaks at 380 cm$^{-1}$ and 340 cm$^{-1}$ are ascribed to the $\nu$O$_{(2)}$=Mo=O$_{(2)}$ and $\delta$O$_{(3)}$–Mo–O$_{(3)}$ deformation modes [10,31]. Moreover, the band at 285 cm$^{-1}$ is ascribed to $\delta$O$_{(1)}$=Mo=O$_{(1)}$ wagging modes, and finally, the band at 260 cm$^{-1}$ is owed to the $\delta$O$_2$–Mo–O$_2$ scissor [10,31]. Concerning the Raman spectrum of MoS$_2$, Figure 5b, the two Raman distinctive peaks

are $E_{2g}$ and $A_{1g}$, situated around 380 cm$^{-1}$ and 400 cm$^{-1}$ that are related to the Mo and S atoms: vibrational in-plane mode and vibrational out-of-plane mode of S atoms, correspondingly [32]. Regarding the WC Raman spectrum, Figure 5c, important peaks appear around 265, 715 and 805 cm$^{-1}$ that coincide with the typical peaks of WC bulk material [33]. Finally, the WS$_2$ Raman spectrum, Figure 5d, displays the two representative peaks of $E_{2g}$ and $A_{1g}$, situated around 360 cm$^{-1}$ and 410 cm$^{-1}$ that are associated with the W and S atoms with the vibrational in-plane mode and the S atoms with the vibrational out-of-plane mode, in that order [34].
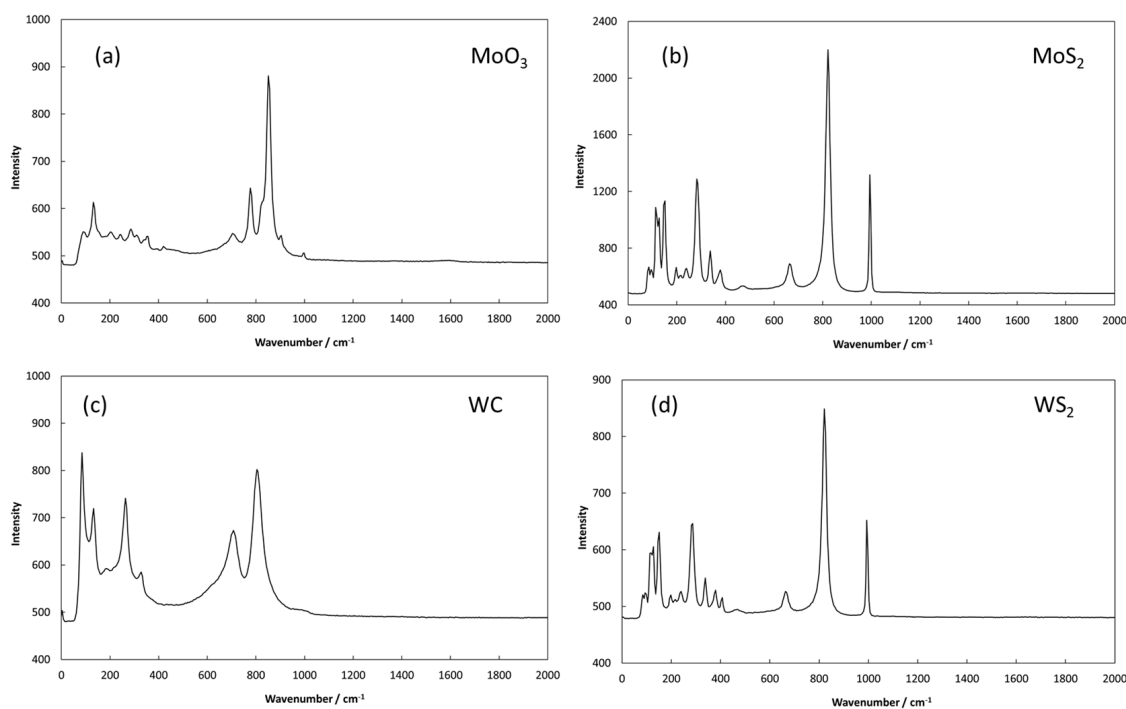


**Figure 5.** Raman spectra of MoO$_3$ (**a**), MoS$_2$ (**b**), WC (**c**) and WS$_2$ (**d**) nanopowders.

### 2.2. Nanolubricants Formulation

Eight nanodispersions were formulated using PAO4 base oil and the aforementioned MoO$_3$, MoS$_2$, WS$_2$ and WC nanopowders. For this aim, the traditional two-step method [35] was utilized, obtaining the following: PAO4 + 0.10 wt% MoO$_3$, PAO4 + 1 wt% MoO$_3$, PAO4 + 0.10 wt% MoS$_2$, PAO4 + 1 wt% MoS$_2$, PAO4 + 0.10 wt% WS$_2$, PAO4 + 1 wt% WS$_2$, PAO4 + 0.10 wt% WC and PAO4 + 1 wt% WC. Therefore, nanolubricants with a high concentration (1 wt%) and low concentration (0.1 wt%) of each nanoparticle were prepared in order to analyze their performance as additives of the PAO4 base oil. The eight potential nanolubricants were sonicated for 4 h through an ultrasonic bath (Fisherbrand, Hampton, USA) working in continuous configuration. Concerning the mass percentage of all the nanodispersions, it was established by using an MC 210P Sartorius balance (0.01 mg readability).

### 2.3. Friction and Wear Analysis: Pure Sliding Conditions

Friction studies with PAO4 and with the MoO$_3$, MoS$_2$, WS$_2$ and WC nanolubricants (0.1 wt% and 1 wt%) were performed on an Anton Paar MCR 302 rheometer (Graz, Austria) equipped with a T-PTD200 tribology cell that contains a H-PTD 200 Peltier hood used for controlling the temperature. For the friction tests, the tribological configuration was ball-on-three pins, the ball being situated on a tube that was powered by the motor of the rheometer and three pins set into a circular box at a 45° angle to the rotating tube. In each tribological run, the ball rotated on the pins below a static force operated by the rheometer that was transferred into three normal forces which acted in a perpendicular way to the pins' surface [36]. The ball (upper pair) had 12.7 mm diameter and a roughness

(Rq) of 0.03 μm, whereas the pins (lower pair) were 6 mm in diameter and height and had a 0.07 μm roughness (Rq). The ball and pins were fabricated from hardened 100Cr6 steel and with a hardness of 62–66 Rockwell C. The pins were completely flooded after adding about 1.3 mL of each studied lubricant. It should be noted that for each lubricant (base oil and nanolubricants), three different replicates were performed to achieve an effective repeatability. Concerning the test conditions, tests were performed with a sliding speed of 0.10 m/s, a friction normal force of 9.43 N and a 393.15 K temperature. More characteristics about the tribometer can be observed in previous research [36–38].

During the friction tests, it was clearly observed that a wear track was produced in the center of the pins. Concerning this wear, an exhaustive evaluation was performed by means of a 3D optical profilometer Sensofar S-Neox quantifying the generated wear with different wear parameters: wear scar diameter (WSD), wear track depth (WTD) or worn area. Therefore, a good evaluation of the wear produced by PAO4 and the different formulated nanolubricants could be determined. It should be noted that the 3D profilometer was also utilized to estimate the worn track roughness (Ra and Rq) of the pins utilized in the tribological tests to demonstrate the anti-wear competence of each nanolubricant. For this aim, ISO 4287 standard was employed applying a Gaussian filter (cut-off: 0.08 mm). Furthermore, the S neox 3D profilometer was calibrated and verified by the manufacturer, following the ISO 25178 standard. Moreover, a Raman microscope WITec alpha300R+ was employed to inspect the worn scars in the pins and perceive information regarding the nanolubricants elements in the worn track (base oil and nanoparticles) and probable wear mechanisms that can appear.

### 2.4. Rolling–Sliding Tests: Stribeck Curves

A ball-on-disc EHD2 tribometer (PCS Instruments, London, UK) was employed to achieve the friction performance of a metal contact pair composed of a carbon chrome steel ball (19.05 mm diameter) and a rotational disc of carbon chrome steel. Both components, disc and ball, were driven with two different electric motors to execute the tests under rolling–sliding conditions. More information involving this equipment can be discovered in previous articles [39]. These types of rolling–sliding friction tests were completed for the PAO4 and the nanolubricants with the best tribological performance in pure sliding conditions under totally flooded lubrication (approximately 125 mL of tested lubricant) at 393.15 K, below a 50 N load generating a maximum Hertz pressure of 0.7 GPa, and a 5% slide-to-roll ratio (*SRR*):

$$SRR(\%) = 2 \times \frac{(U_{disc} - U_{ball})}{(U_{disc} + U_{ball})} \times 100 \tag{1}$$

with $U_{disc}$ and $U_{ball}$ being the disc and ball speeds in the tribological point contact correspondingly, whereas the entrainment speed ($U_s$) is

$$U_S = \frac{(U_{disc} + U_{ball})}{2} \tag{2}$$

The friction characteristics of $MoS_2$ nanolubricants and PAO4 base oil were studied through Stribeck curves using three different balls (two rough and one smooth, Figure 6) for an SRR value of 5%. The same entrainment speed conditions (ramp of 0.05 to 2 m/s) were utilized for all tribological tests. The friction coefficient was calculated as the average of those reached from two separate tribological studies, the first ramp improving speed and the second one lowering speed. The assets of the disc and balls (Table 1) were provided by the supplier, whereas the balls' surface roughness was determined with the 3D optical profilometer (Table 1).
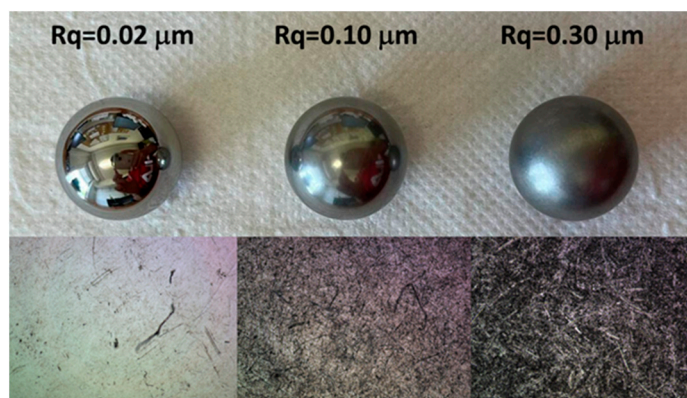
**Figure 6.** Smooth and rough balls tested in rolling–sliding friction studies.

**Table 1.** Main physical properties of disc and balls utilized in rolling–sliding tests.

| Parameters | Steel Disc | Steel Balls | | |
| --- | --- | --- | --- | --- |
| | | Smooth | Rough 1 | Rough 2 |
| Elastic modulus/GPa | 210 | 210 | 210 | 210 |
| Poisson coefficient/GPa | 0.29 | 0.29 | 0.29 | 0.29 |
| Diameter/mm | 100 | 19.05 | 19.05 | 19.05 |
| Surface roughness, Rq/nm | 20 | 20 | 100 | 300 |

## 3. Results

### 3.1. Pure Sliding Tests: Friction and Wear Results

The average coefficients of friction ($\mu$) found under pure sliding for PAO4 and the eight nanolubricants of $MoO_3$, $MoS_2$, $WS_2$ and WC with PAO4 base oil are displayed in Figure 7 and Table 2. It can be evidently observed that for all the prepared nanolubricants, the attained friction coefficients were smaller than that of the unadditivated PAO4. The biggest friction reductions were achieved for the $MoS_2$ nanolubricants and in particular for the low concentration (0.1 wt%). Thus, the lowest mean friction coefficient was 0.067, obtained with the 0.1 wt% $MoS_2$ nanolubricant, while the value achieved for the PAO4 base oil was 0.185. Therefore, a maximum of 64% friction decrease due to the 0.1 wt% $MoS_2$ NPs was reached. Concerning the other nanoadditives, maximum friction reductions of 29% (1 wt% $MoO_3$), 51% (1 wt% $WS_2$) and 22% (0.1 wt% WC) were found in comparison with the PAO4 base oil. Therefore, for nanolubricants that contain $MoO_3$ and $WS_2$, the optimal friction behavior appeared with the highest mass concentration (1 wt%), whereas in the case of $MoS_2$ and WC, the low concentration (0.1 wt%) was the optimal. It is also clearly observed in both Table 2 and Figure 7 that the $MoS_2$ nanolubricants (0.1 and 1 wt%) showed the best friction performance.
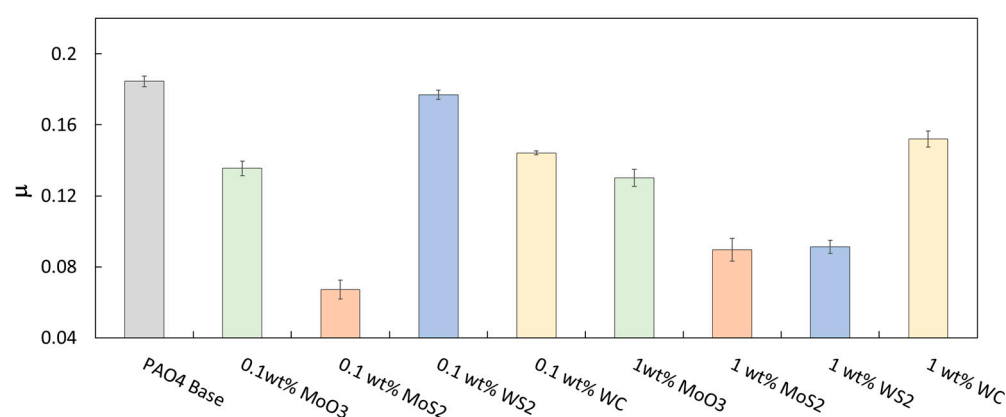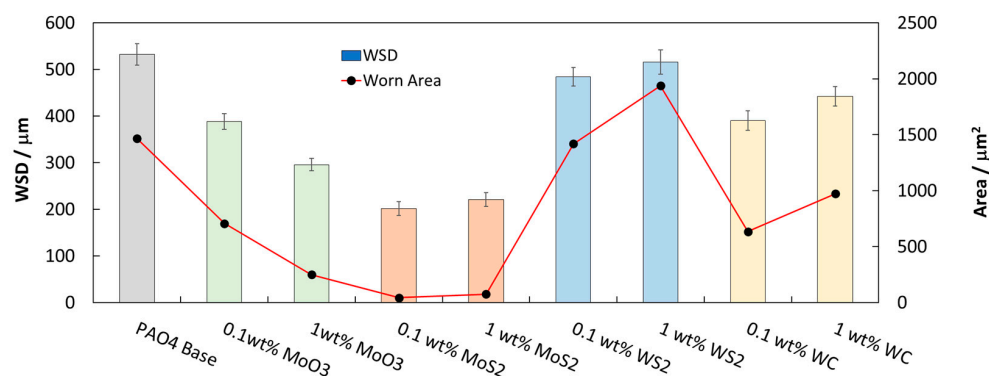


**Figure 7.** Difference among friction coefficients ($\mu$) achieved with PAO4 and formulated nanolubricants.

**Table 2.** Mean friction coefficients, μ, and average wear parameters: width (WSD), depth (WTD), and area for all the tested nanolubricants and PAO4 base oil.

| Lubricant | μ | σ | WSD/μm | σ/μm | WTD/μm | σ/μm | Area/μm$^2$ | σ/μm$^2$ |
|---|---|---|---|---|---|---|---|---|
| PAO4 | 0.1845 | 0.0029 | 532 | 23 | 4.70 | 0.49 | 1467 | 184 |
| +0.1 wt% MoO$_3$ | 0.1355 | 0.0040 | 388 | 17 | 2.37 | 0.32 | 707.1 | 102 |
| +1 wt% MoO$_3$ | 0.1302 | 0.0048 | 296 | 13 | 1.44 | 0.13 | 250.3 | 56.8 |
| +0.1 wt% MoS$_2$ | 0.06713 | 0.00543 | 201 | 15 | 0.30 | 0.04 | 44.20 | 10.5 |
| +1 wt% MoS$_2$ | 0.08971 | 0.00643 | 221 | 15 | 0.45 | 0.08 | 75.78 | 12.7 |
| +0.1 wt% WS$_2$ | 0.1770 | 0.0027 | 484 | 20 | 4.35 | 0.51 | 1420 | 196 |
| +1 wt% WS$_2$ | 0.09125 | 0.0037 | 516 | 26 | 5.37 | 0.65 | 1939 | 230 |
| +0.1 wt% WC | 0.1442 | 0.0010 | 390 | 21 | 2.52 | 0.33 | 634.3 | 106 |
| +1 wt% WC | 0.1521 | 0.0044 | 442 | 21 | 3.58 | 0.52 | 972.4 | 121 |

Concerning the wear generated in the pins (lower specimen) during the friction tribological tests, it is observed in Figure 8 and Table 2 that all the formulated nanolubricants demonstrated improved antiwear characteristics in comparison to PAO4 without additives, in terms of WSD. It is especially remarkable that the MoS$_2$ nanolubricants obtained the best antiwear properties (Figures 9 and 10), with width decreases of 62% and 58% for 0.1 wt% and 1 wt% in MoS$_2$, respectively. Moreover, in terms of the worn area, reductions of 97% and 95% for 0.1 wt% and 1 wt% in MoS$_2$ were reached, respectively, in comparison to the worn area with the PAO4 base oil. Additionally, wear reductions were also obtained for the following nanolubricants in terms of width and area, respectively: 0.1 wt% MoO$_3$ (27% and 52%), 1 wt% MoO$_3$ (39% and 82%), 0.1 wt% WS$_2$ (9% and 3%), 0.1 wt% WC (27% and 57%) and 1 wt% WC (17% and 34%).



**Figure 8.** Comparison between wear scar diameters and worn areas found with PAO4 and nanolubricants. For WSD values: PAO in grey, MoO$_3$ in green, MOS$_2$ in orange, WS$_2$ in blue and WC in yellow.

Roughness analyses (Ra and Rq) on pins after friction tests expose that the worn tracks oiled with nanolubricants with MoS$_2$ NPs report decreased roughness in comparison to PAO4 (Table 3). Hence, an Ra value of 31.8 nm was obtained for the worn surfaces tested with PAO4, but those tried with the nanolubricant PAO4 + 0.1 wt% MoS$_2$ reached the minimal Ra value (10.1 nm), indicating a roughness drop of 68%. These facts suggest that owing to the occurrence of the NPs in the tribological contact, a more consistent wear surface is observed after friction tests.

Mappings of Raman in the worn pins were performed to acquire knowledge on the distribution of NPs in worn surfaces after friction tests. Earlier, the Raman spectra of the different elements of the nanolubricants were obatined: PAO4 base oil (Figure 2b) and nanoadditives (Figure 5) to distinguish the lubricant elements in the mapping. Consequently, mappings of the worn pins lubricated with the nanolubricants with the greatest antiwear behavior (MoO$_3$ and MoS$_2$ NPs) were carried out using the Raman microscope to

find the role that NPs play in reducing the produced wear in the pins. Figure 11 shows the Raman mapping of the worn scar oiled with the PAO4 + 1 wt% $MoO_3$ nanolubricant, with the important areas in green and red, which match with the spectrum found for PAO4 and $MoO_3$, respectively. This fact suggests that mending and small tribofilm formation mechanisms occur on the worn pins, owing to $MoO_3$ nanoparticles. Sun et al. [40] also studied the tribological performance of this type of NP ($MoO_3$) but as additives of a water-based solution. These authors concluded that the key tribological mechanism of $MoO_3$ NPs is the creation of a lubricant film on surfaces, owing to the electron transfer and deposition, the $MoO_3$ being reduced to $MoO_2$, and the Fe from the recently formed surface was oxidized to $Fe(OH)_3$. Additionally, they observed that nano-$MoO_3$ was placed in the grooves of the friction surfaces to fulfill the gullies of the worn surfaces.
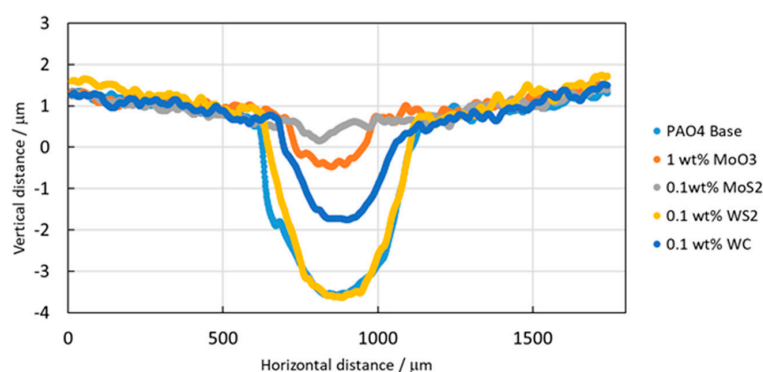


**Figure 9.** Comparison between cross-section profiles of worn pins lubricated with PAO4 and the ideal nanolubricants formulated with the different NPs.
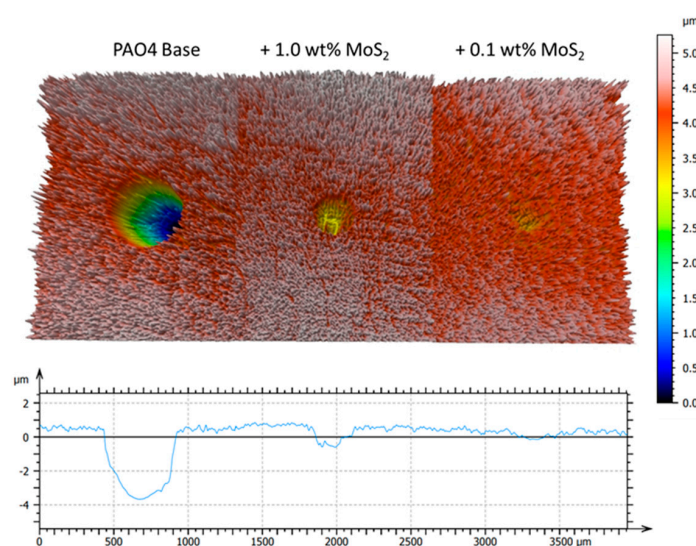


**Figure 10.** 3D and 2D profiles of worn pins tested with PAO4 and the optimal $MoS_2$ nanolubricants.

Furthermore, Figure 12 displays the mapping Raman of the surface tested with 0.1 wt% $MoS_2$ nanolubricant, observing green areas that corresponds to PAO4, very uniform red areas that are associated with the $MoS_2$ placed in the grooves of the friction surfaces to fulfill the gullies of the surfaces and blue areas that are attributed to the formed iron oxides. Taking into account these facts and the lists of these NPs as additives, it can be suggested that the enhanced friction and wear properties of $MoS_2$ nanolubricants related to the PAO4 base oil could be ascribed to the adequate exfoliation on NPs at the tribological area [41] (mending effect) and the creation of important tribofilms [42]. This exfoliation and the subsequent distortion led to the existence of $MoS_2$ NPs in the asperity contacts of tribopairs. The tribofilm mechanisms of $MoS_2$ NPs were previously demonstrated by Xu et al. [43] in their research.

**Table 3.** Average roughness values, Ra and Rq, in worn pins tested with all lubricants.

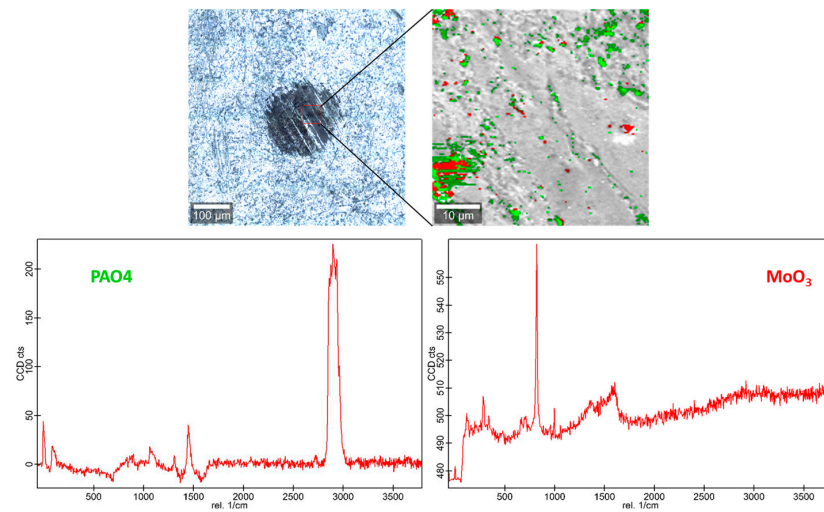| Lubricant | Ra/nm | σ | Rq/nm | σ |
|---|---|---|---|---|
| PAO4 | 31.8 | 2.9 | 41.4 | 4.2 |
| +0.1 wt% $MoO_3$ | 27.5 | 2.1 | 32.7 | 3.3 |
| +0.1 wt% $MoS_2$ | 10.1 | 1.3 | 13.0 | 1.5 |
| +0.1 wt% $WS_2$ | 23.6 | 2.3 | 28.2 | 2.5 |
| +0.1 wt% WC | 21.3 | 1.9 | 26.2 | 1.8 |
| +1 wt% $MoO_3$ | 16.2 | 1.4 | 20.1 | 2.0 |
| +1 wt% $MoS_2$ | 11.1 | 1.2 | 13.9 | 1.4 |
| +1 wt% $WS_2$ | 29.3 | 2.6 | 34.9 | 3.7 |
| +1 wt% WC | 27.5 | 2.3 | 31.2 | 3.0 |



**Figure 11.** Mapping Raman of worn surface tested with 1 wt% $MoO_3$ nanolubricant.

In metal sulfides, sulfur play an important role in the interface between nanoparticles and lubricant molecules because the heat generated by friction and elevated contact pressure conduct to a possible tribo-chemical reaction between nanoparticles and their environments (lubricant, substrate, etc.) [44]. Consequently, a tribofilm can be formed on the friction surface. In this case, the tribofilm adsorption is formed by $MoS_2$ NPs, the lubricant and their chemically bonded compounds. Usually, the tribofilm mechanism (Figure 13) is the most general model to explain the antiwear and friction reduction behavior of nanolubricants. Most researchers assigned the better lubrication performance of nanolubricants to the fact that NPs are set on rubbing surfaces and forming a protective film.
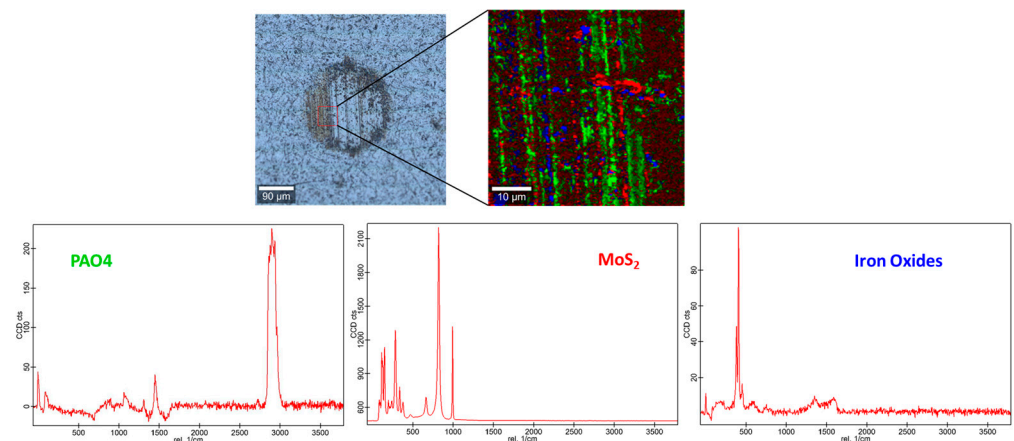


**Figure 12.** Mapping Raman of worn surface tested with 0.1 wt% $MoS_2$ nanolubricant.
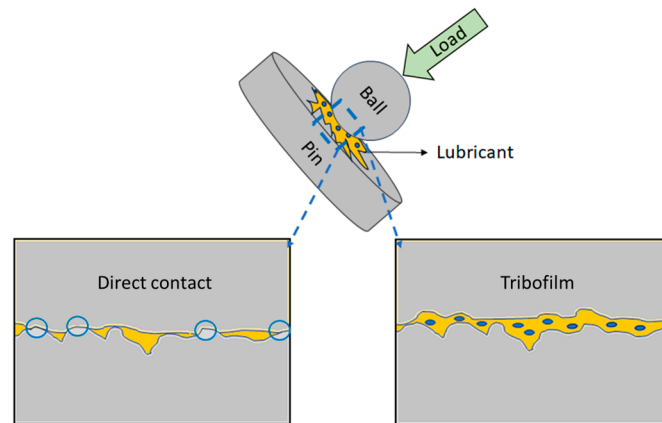
**Figure 13.** Representation of the tribological mechanism of tribofilm in the studied tribological pair.

### 3.2. Results Found in Rolling–Sliding Tests

Tribological studies under rolling–sliding for PAO4 and the formulated 0.1 and 1 wt% MoS$_2$ nanolubricants were made at 120 °C as the sliding tests and with SRR of 5%, achieving the Stribeck curves (Figures 14 and 15). In this research, Stribeck curves are obtained by drawing the friction coefficient against specific film thickness, $\Lambda$, which is designed by

$$\Lambda = \frac{h_t}{Rq} \tag{3}$$

with $h_t$ being the theoretical central film thickness, and Rq is the mean roughness of the two tribological surfaces given by $Rq = \sqrt{(Rq_{disc})^2 + (Rq_{ball})^2}$. The central film thickness ($h_t$) at the 120 °C temperature was estimated with Hamrock and Downson's equation [45], considering different parameters such as materials and lubricant properties and operational conditions. For the estimation of $h_t$, the PAO6 pressure−viscosity coefficient was utilized [46]. Concerning the viscosities, a Stabinger SVM3000 (Anton Paar, Graz, Austria) was utilized to determine them up to 100 °C (Table S1). Furthermore, Vogel−Fulcher−Tammann equation [46] was used to correlate the viscosities of the different studied lubricants to achieve the dynamic viscosity of all nanolubricants and the PAO4 base oil at 120 °C from this equation, due to the fact that the viscosimeter can measure the viscosity just up to 100 °C.



**Figure 14.** *Cont.*
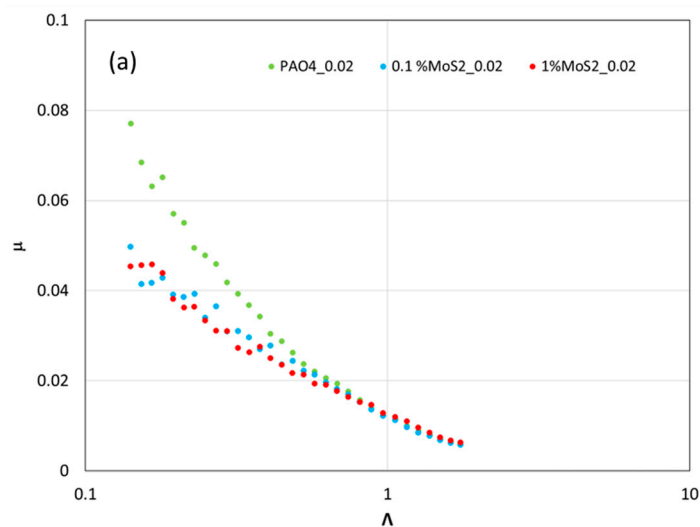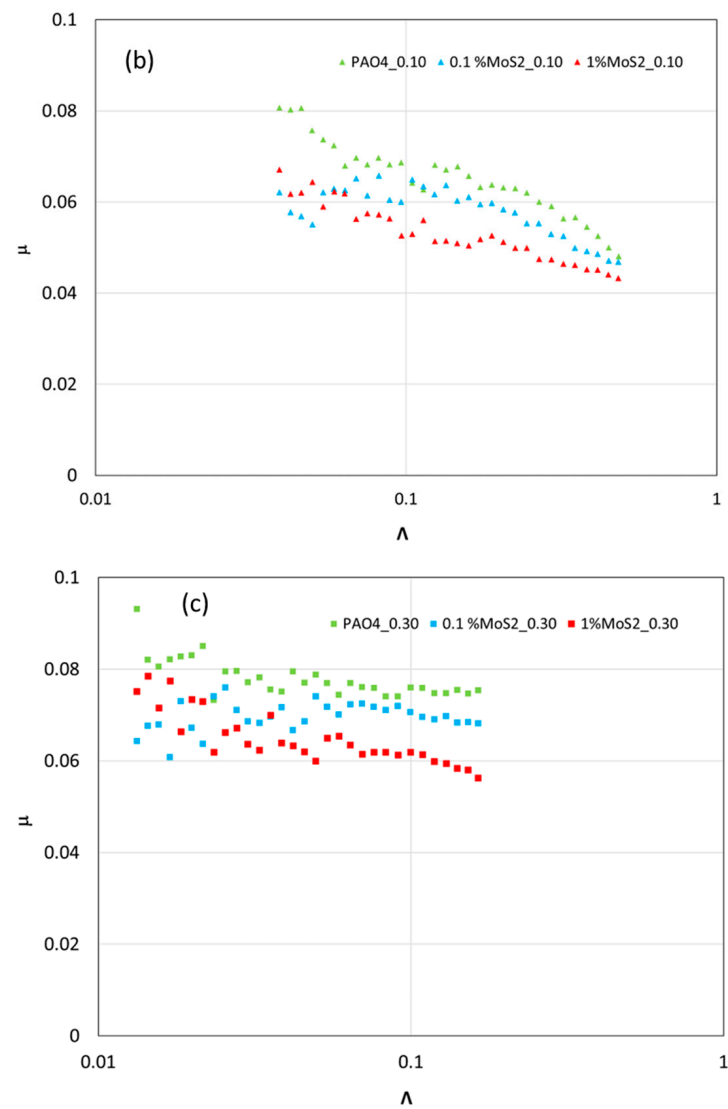
**Figure 14.** Stribeck curves of PAO4 and MoS$_2$ nanolubricants tested at 120 °C for the balls with three different degrees of roughness: 0.02 μm (**a**), 0.10 μm (**b**) and 0.30 μm (**c**).
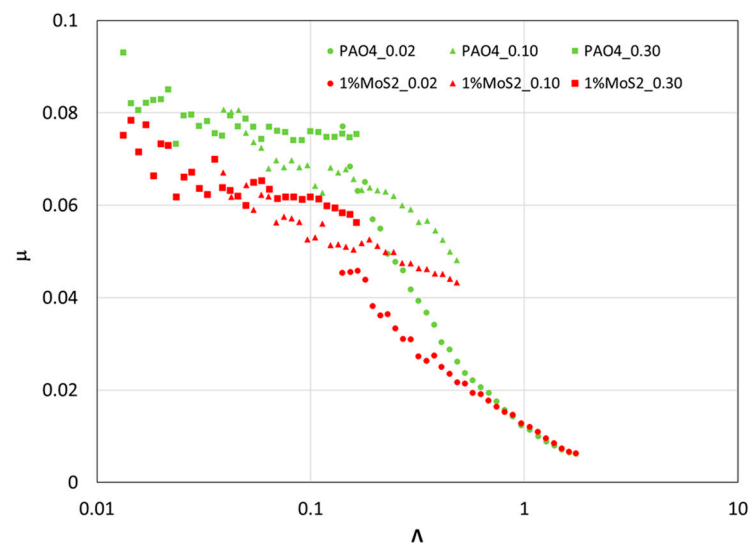


**Figure 15.** Full Stribeck curves of PAO4 (green) and PAO4 + 1 wt% MoS$_2$ nanolubricant (red) tested with each ball (0.02 μm, 0.10 μm and 0.30 μm) at 120 °C and 5% SRR.

All the obtained Stribeck curves are plotted in Figures 14 and 15 for PAO4 base oil and both MoS$_2$ nanolubricants with balls with three different degrees of roughness (Table 1). As it was presumed, in tribological tests, the friction coefficient rises when the roughness of the balls increases. Figure 14 represents separately the friction performance of the three tested lubricants (PAO4 base oil, 0.1 and 1 wt% MoS$_2$ nanolubricants) for each tested ball with diverse roughness. It can be evidently seen that the reached friction coefficients are quite decreased for the two MoS$_2$ nanolubricants compared to the PAO4 base oil. In this case, the best friction behavior was very similar for both MoS$_2$ nanolubricants, although the 0.1 wt% MoS$_2$ nanolubricant seems to be a very little better, and that is the reason why just the full Stribeck curves corresponding to PAO4 without additives and 0.1 wt% MoS$_2$ nanolubricant are represented in Figure 15. The achieved results of Figure 15 for each different ball are very noteworthy because it can be found that for high specific film thicknesses and therefore high speeds, the coefficient of friction is quite comparable for both MoS$_2$ nanolubricants and the PAO4 base oil. On the contrary, at very low speeds, the consequence of the MoS$_2$ NPs addition is vital, helping to significantly reduce the friction when the hydrodynamic effect is insignificant (low speeds).

As it is known, a Stribeck curve is divided in diverse regimes of lubrication: boundary lubrication, mixed lubrication, elastohydrodynamic and hydrodynamic and full film lubrication. Depending on the different criteria in the literature, the boundary lubrication appears when $\Lambda < 1$, mixed if $1 < \Lambda < 3$, elastohydrodynamic (EHL) if $\Lambda > 3$ and $\Lambda > 5$ for full film. Regarding the achieved results displayed in Figure 15, the obtained $\Lambda$ values vary between a minimum of around 0.02 (for the roughest ball) to about 1.8 (the ball with lowest roughness). Consequently, based on earlier articles, boundary film lubrication ought to happen for all the examined balls, while mixed and full film lubrication only ought to appear for the smoothest ball at high speeds.

Furthermore, the wear created in disc and balls in the rolling–sliding tests can scarcely be determined because it is almost non-present. Nonetheless, the authors were able to measure the width of the wear track (WTW) on the balls with the highest roughness (0.3 μm). As Figure 16 shows, the wear generated in the balls lubricated with MoS$_2$ nanolubricants is lower than that reached with the PAO4 base oil. Specifically, reductions in the WTW of 17% and 8% were achieved for 0.10 wt% MoS$_2$ and 1 wt% MoS$_2$, respectively. Therefore, these results are in accordance with those obtained for the pure sliding conditions.
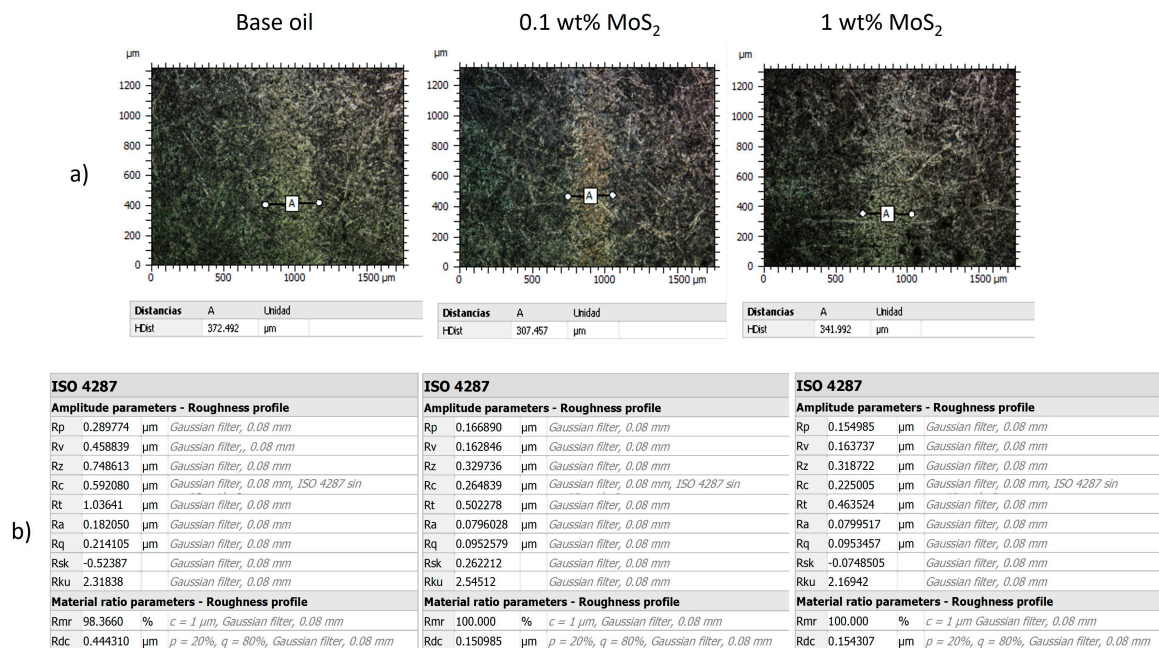
**Base oil**

a)

| Distancias | A | Unidad |
|---|---|---|
| HDist | 372.492 | μm |

**0.1 wt% MoS$_2$**

| Distancias | A | Unidad |
|---|---|---|
| HDist | 307.457 | μm |

**1 wt% MoS$_2$**

| Distancias | A | Unidad |
|---|---|---|
| HDist | 341.992 | μm |

b)

**ISO 4287 — Base oil**

**Amplitude parameters - Roughness profile**

| | | | |
|---|---|---|---|
| Rp | 0.289774 | μm | *Gaussian filter, 0.08 mm* |
| Rv | 0.458839 | μm | *Gaussian filter,, 0.08 mm* |
| Rz | 0.748613 | μm | *Gaussian filter, 0.08 mm* |
| Rc | 0.592080 | μm | *Gaussian filter, 0.08 mm, ISO 4287 sin* |
| Rt | 1.03641 | μm | *Gaussian filter, 0.08 mm* |
| Ra | 0.182050 | μm | *Gaussian filter, 0.08 mm* |
| Rq | 0.214105 | μm | *Gaussian filter, 0.08 mm* |
| Rsk | -0.52387 | | *Gaussian filter, 0.08 mm* |
| Rku | 2.31838 | | *Gaussian filter, 0.08 mm* |

**Material ratio parameters - Roughness profile**

| | | | |
|---|---|---|---|
| Rmr | 98.3660 | % | *c = 1 μm, Gaussian filter, 0.08 mm* |
| Rdc | 0.444310 | μm | *p = 20%, q = 80%, Gaussian filter, 0.08 mm* |

**ISO 4287 — 0.1 wt% MoS$_2$**

**Amplitude parameters - Roughness profile**

| | | | |
|---|---|---|---|
| Rp | 0.166890 | μm | *Gaussian filter, 0.08 mm* |
| Rv | 0.162846 | μm | *Gaussian filter, 0.08 mm* |
| Rz | 0.329736 | μm | *Gaussian filter, 0.08 mm* |
| Rc | 0.264839 | μm | *Gaussian filter, 0.08 mm, ISO 4287 sin* |
| Rt | 0.502278 | μm | *Gaussian filter, 0.08 mm* |
| Ra | 0.0796028 | μm | *Gaussian filter, 0.08 mm* |
| Rq | 0.0952579 | μm | *Gaussian filter, 0.08 mm* |
| Rsk | 0.262212 | | *Gaussian filter, 0.08 mm* |
| Rku | 2.54512 | | *Gaussian filter, 0.08 mm* |

**Material ratio parameters - Roughness profile**

| | | | |
|---|---|---|---|
| Rmr | 100.000 | % | *c = 1 μm, Gaussian filter, 0.08 mm* |
| Rdc | 0.150985 | μm | *p = 20%, q = 80%, Gaussian filter, 0.08 mm* |

**ISO 4287 — 1 wt% MoS$_2$**

**Amplitude parameters - Roughness profile**

| | | | |
|---|---|---|---|
| Rp | 0.154985 | μm | *Gaussian filter, 0.08 mm* |
| Rv | 0.163737 | μm | *Gaussian filter, 0.08 mm* |
| Rz | 0.318722 | μm | *Gaussian filter, 0.08 mm* |
| Rc | 0.225005 | μm | *Gaussian filter, 0.08 mm, ISO 4287 sin* |
| Rt | 0.463524 | μm | *Gaussian filter, 0.08 mm* |
| Ra | 0.0799517 | μm | *Gaussian filter, 0.08 mm* |
| Rq | 0.0953457 | μm | *Gaussian filter, 0.08 mm* |
| Rsk | -0.0748505 | | *Gaussian filter, 0.08 mm* |
| Rku | 2.16942 | | *Gaussian filter, 0.08 mm* |

**Material ratio parameters - Roughness profile**

| | | | |
|---|---|---|---|
| Rmr | 100.000 | % | *c = 1 μm Gaussian filter, 0.08 mm* |
| Rdc | 0.154307 | μm | *p = 20%, q = 80%, Gaussian filter, 0.08 mm* |

**Figure 16.** WTW (**a**) and roughness (**b**) observed after rolling–sliding tests with PAO4 base oil, 0.1 wt% MoS$_2$ and 1 wt% MoS$_2$ nanolubricants.

In addition, the roughness of the aforementioned balls after the rolling–sliding tests were measured with the 3D optical Profilometer S-Neox and compared with the untested balls and the balls lubricated with the base oil and the $MoS_2$ nanolubricants (Figure 16). Thus, an Rq value of 0.304 µm was obtained for the untested ball, 0.214 µm for the PAO4 and 0.095 µm for both 0.1 and 1 wt% $MoS_2$ nanolubricants, which led to an Rq roughness decrease of 56% compared to the ball lubricated with the PAO4 base oil. These results are also in accordance with the roughness analysis of pins in pure sliding tests.

## 4. Conclusions

Eight nanolubricants based on PAO4 low-viscosity oil and $MoO_3$, $MoS_2$, $WS_2$ and WC NPs as antifriction and antiwear additives were tribologically characterized. The conclusions of this research can be summed up as follows:

- The friction coefficients reached with all nanolubricants are minor compared to those obtained for the PAO4 oil for the tribological tests (pure sliding and rolling/sliding).
- The largest friction decreases in the pure sliding tests were obtained for the $MoS_2$ nanolubricants (0.10 wt%), with a maximum 64% friction reduction.
- All the nanolubricants demonstrated an improved antiwear performance in comparison to PAO4. $MoS_2$ nanolubricants reached the best antiwear behavior with width reductions of 62% and 58% for 0.1 wt% and 1 wt% in $MoS_2$, respectively.
- From the roughness analysis and Raman mappings of worn pins tested in pure sliding circumstances, it is suggested that the lubrication mechanism of $MoS_2$ nanolubricants might be explained by the creation of a tribofilm and the mending effects.
- Concerning the rolling/sliding tests (small slide-to-roll ratio (SRR)), the antifriction capability of $MoS_2$ NPs is remarkable at low speeds, indicating that the use of NPs is vital in boundary lubrication.

## References

1. Holmberg, K.; Erdemir, A. The impact of tribology on energy use and $CO_2$ emission globally and in combustion engine and electric cars. *Tribol. Int.* **2019**, *135*, 389–396. [CrossRef]
2. Gupta, A. Characterization of Engine and Transmission Lubricants for Electric, Hybrid, and Plug-In Hybrid Vehicles. Ph.D. Thesis, Ohio State University, Columbus, OH, USA, 2012.
3. Aguilar-Rosas, O.A.; Alvis-Sánchez, J.A.; Tormos, B.; Marín-Santibáñez, B.M.; Pérez-González, J.; Farfan-Cabrera, L.I. Enhancement of low-viscosity synthetic oil using graphene nanoparticles as additives for enduring electrified tribological environments. *Tribol. Int.* **2023**, *188*, 108848. [CrossRef]

4.  Mariño, F.; Liñeira del Río, J.M.; López, E.R.; Fernández, J. Chemically modified nanomaterials as lubricant additive: Time stability, friction, and wear. *J. Mol. Liq.* **2023**, *382*, 121913. [CrossRef]

5.  Ahmed Abdalglil Mustafa, W.; Dassenoy, F.; Sarno, M.; Senatore, A. A review on potentials and challenges of nanolubricants as promising lubricants for electric vehicles. *Lubr. Sci.* **2022**, *34*, 1–29. [CrossRef]

6.  Gulzar, M.; Masjuki, H.H.; Kalam, M.A.; Varman, M.; Zulkifli, N.W.M.; Mufti, R.A.; Zahid, R. Tribological performance of nanoparticles as lubricating oil additives. *J. Nanopart. Res.* **2016**, *18*, 223. [CrossRef]

7.  Liñeira del Río, J.M.; Mariño, F.; López, E.R.; Gonçalves, D.E.P.; Seabra, J.H.O.; Fernández, J. Tribological enhancement of potential electric vehicle lubricants using coated $TiO_2$ nanoparticles as additives. *J. Mol. Liq.* **2023**, *371*, 121097. [CrossRef]

8.  Demas, N.; Timofeeva, E.; Routbort, J.; Fenske, G. Tribological Effects of BN and $MoS_2$ Nanoparticles Added to Polyalphaolefin Oil in Piston Skirt/Cylinder Liner Tests. *Tribol. Lett.* **2012**, *47*, 91–102. [CrossRef]

9.  Kalin, M.; Kogovšek, J.; Remškar, M. Mechanisms and improvements in the friction and wear behavior using $MoS_2$ nanotubes as potential oil additives. *Wear* **2012**, *280–281*, 36–45. [CrossRef]

10. Lee, E.L.; Wachs, I.E. In Situ Spectroscopic Investigation of the Molecular and Electronic Structures of $SiO_2$ Supported Surface Metal Oxides. *J. Phys. Chem. C* **2007**, *111*, 14410–14425. [CrossRef]

11. Nagarajan, T.; Khalid, M.; Sridewi, N.; Jagadish, P.; Shahabuddin, S.; Muthoosamy, K.; Walvekar, R. Tribological, oxidation and thermal conductivity studies of microwave synthesised molybdenum disulfide ($MoS_2$) nanoparticles as nano-additives in diesel based engine oil. *Sci. Rep.* **2022**, *12*, 14108. [CrossRef]

12. Mousavi, S.B.; Heris, S.Z.; Estellé, P. Experimental comparison between ZnO and $MoS_2$ nanoparticles as additives on performance of diesel oil-based nano lubricant. *Sci. Rep.* **2020**, *10*, 5813. [CrossRef]

13. Yi, M.; Qiu, J.; Xu, W. Tribological performance of ultrathin $MoS_2$ nanosheets in formulated engine oil and possible friction mechanism at elevated temperatures. *Tribol. Int.* **2022**, *167*, 107426. [CrossRef]

14. Yu, R.; Liu, J.; Zhou, Y. Experimental Study on Tribological Property of $MoS_2$ Nanoparticle in Castor Oil. *J. Tribol.* **2019**, *141*, 102001. [CrossRef]

15. Ouyang, T.; Lei, W.; Tang, W.; Shen, Y.; Mo, C. Experimental investigation of the effect of $IF-WS_2$ as an additive in castor oil on tribological property. *Wear* **2021**, *486–487*, 204070. [CrossRef]

16. Srinivas, V.; Thakur, R.N.; Jain, A.K.; Saratchandra Babu, M. Physicochemical properties and tribological performance of motorbike lubricant dispersed with surface-modified $WS_2$ nanoparticles. *Proc. Inst. Mech. Eng. Part J J. Eng. Tribol.* **2019**, *233*, 1379–1388. [CrossRef]

17. Guan, Z.; Zhang, P.; Florian, V.; Wu, Z.; Zeng, D.; Liu, J.; Wang, B.; Tu, X.; Li, S.; Li, W. Preparation and tribological behaviors of magnesium silicate hydroxide-$MoS_2$ nanoparticles as lubricant additive. *Wear* **2022**, *492–493*, 204237. [CrossRef]

18. Srivastava, J.; Nandi, T.; Trivedi, R.K. Experimental Investigations on Thermophysical, Tribological and Rheological Properties of $MoS_2$ and $WS_2$ Based Nanolubricants with Castor Oil as Base Lubricant. *Tribol. Ind.* **2023**, *45*, 591–603. [CrossRef]

19. Sepehrnia, M.; Maleki, H.; Forouzandeh Behbahani, M. Tribological and rheological properties of novel $MoO_3$-GO-MWCNTs/5W30 ternary hybrid nanolubricant: Experimental measurement, development of practical correlation, and artificial intelligence modeling. *Powder Technol.* **2023**, *421*, 118389. [CrossRef]

20. Zhang, X.; Wan, S.; Pu, J.; Wang, L.; Liu, X. Highly hydrophobic and adhesive performance of graphene films. *J. Mater. Chem.* **2011**, *21*, 12251–12258. [CrossRef]

21. Nyamekye, C.K.A.; Bobbitt, J.M.; Zhu, Q.; Smith, E.A. The evolution of total internal reflection Raman spectroscopy for the chemical characterization of thin films and interfaces. *Anal. Bioanal. Chem.* **2020**, *412*, 6009–6022. [CrossRef] [PubMed]

22. Okubo, H.; Tadokoro, C.; Hirata, Y.; Sasaki, S. In Situ Raman Observation of the Graphitization Process of Tetrahedral Amorphous Carbon Diamond-Like Carbon under Boundary Lubrication in Poly-Alpha-Olefin with an Organic Friction Modifier. *Tribol. Online* **2017**, *12*, 229–237. [CrossRef]

23. Klinbumrung, A.; Thongtem, T.; Thongtem, S. Characterization of Orthorhombic Characterization of Orthorhombic α-$MoO_3$ Microplates Produced by a Microwave Plasma Process. *J. Nanomater.* **2012**, *2012*, 930763. [CrossRef]

24. Siciliano, T.; Tepore, A.; Filippo, E.; Micocci, G.; Tepore, M. Characteristics of molybdenum trioxide nanobelts prepared by thermal evaporation technique. *Mater. Chem. Phys.* **2009**, *114*, 687–691. [CrossRef]

25. Penyediaan, Z.; Sulfida, L.; Peralihan, B.; Nano, M.; Kaedah, H.; Pua, F.L.; Chia, C.-h.; Zakaria, S.; Liew, T.-K.; Yarmo, A.; et al. Preparation of Transition Metal Sulfide Nanoparticles via Hydrothermal Route. *Sains Malays.* **2010**, *39*, 243–248.

26. Philias, J.M.; Marsan, B. FTIR spectroscopic study and thermal and electrical properties of polymer electrolytes containing a cesium thiolate/disulfide redox couple. *Electrochim. Acta* **1999**, *44*, 2351–2363. [CrossRef]

27. Philip, D.; Eapen, A.; Aruldhas, G. Vibrational and Surface Enhanced Raman Scattering Spectra of Sulfamic Acid. *J. Solid State Chem.* **1995**, *116*, 217–223. [CrossRef]

28. Hoffmann, P.; Galindo, H.; Zambrano, G.; Rincón, C.; Prieto, P. FTIR studies of tungsten carbide in bulk material and thin film samples. *Mater. Charact.* **2003**, *50*, 255–259. [CrossRef]

29. Wu, J.; Yue, G.; Xiao, Y.; Huang, M.; Lin, J.; Fan, L.; Lan, Z.; Lin, J.-Y. Glucose Aided Preparation of Tungsten Sulfide/Multi-Wall Carbon Nanotube Hybrid and Use as Counter Electrode in Dye-Sensitized Solar Cells. *ACS Appl. Mater. Interfaces* **2012**, *4*, 6530–6536. [CrossRef]

30. Malyala, L.; Rani, J. $WS_2$/Graphene Composite as Cathode for Rechargeable Aluminum-Dual Ion Battery. *J. Electrochem. Soc.* **2020**, *167*, 070501. [CrossRef]

31. Handzlik, J. DFT study of molybdena–silica system—A selection of density functionals based on their performance in thermochemistry of molybdenum compounds. *Chem. Phys. Lett.* **2009**, *469*, 140–144. [CrossRef]

32. Lee, C.; Yan, H.; Brus, L.E.; Heinz, T.F.; Hone, J.; Ryu, S. Anomalous Lattice Vibrations of Single- and Few-Layer MoS$_2$. *ACS Nano* **2010**, *4*, 2695–2700. [CrossRef]

33. Yan, Y.; Xia, B.; Qi, X.; Wang, H.; Xu, R.; Wang, J.-Y.; Zhang, H.; Wang, X. Nano-tungsten carbide decorated graphene as co-catalysts for enhanced hydrogen evolution on molybdenum disulfide. *Chem. Commun.* **2013**, *49*, 4884–4886. [CrossRef]

34. Berkdemir, A.; Gutiérrez, H.R.; Botello-Méndez, A.R.; Perea-López, N.; Elías, A.L.; Chia, C.-I.; Wang, B.; Crespi, V.H.; López-Urías, F.; Charlier, J.-C.; et al. Identification of individual and few layers of WS$_2$ using Raman Spectroscopy. *Sci. Rep.* **2013**, *3*, 1755. [CrossRef]

35. Liñeira del Río, J.M.; López, E.R.; Fernández, J.; García, F. Tribological properties of dispersions based on reduced graphene oxide sheets and trimethylolpropane trioleate or PAO 40 oils. *J. Mol. Liq.* **2019**, *274*, 568–576. [CrossRef]

36. Heyer, P.; Läuger, J. Correlation between friction and flow of lubricating greases in a new tribometer device. *Lubr. Sci.* **2009**, *21*, 253–268. [CrossRef]

37. Vallejo, J.P.; Liñeira del Río, J.M.; Fernández, J.; Lugo, L. Tribological performance of silicon nitride and carbon black Ionanofluids based on 1-ethyl-3-methylimidazolium methanesulfonate. *J. Mol. Liq.* **2020**, *319*, 114335. [CrossRef]

38. Läuger, J.; Pondicherry, K. New Insights into the Use of a Rotational Rheometer as Tribometer. *Annu. Trans. Nord. Rheol. Soc.* **2017**, *25*, 333–340.

39. Liñeira del Río, J.M.; López, E.R.; González Gómez, M.; Yáñez Vilar, S.; Piñeiro, Y.; Rivas, J.; Gonçalves, D.E.P.; Seabra, J.H.O.; Fernández, J. Tribological Behavior of Nanolubricants Based on Coated Magnetic Nanoparticles and Trimethylolpropane Trioleate Base Oil. *Nanomaterials* **2020**, *10*, 683. [CrossRef] [PubMed]

40. Sun, J.; Meng, Y.; Zhang, B. Tribological Behaviors and Lubrication Mechanism of Water-based MoO3 Nanofluid during Cold Rolling Process. *J. Manuf. Process.* **2021**, *61*, 518–526. [CrossRef]

41. Lahouij, I.; Dassenoy, F.; Vacher, B.; Martin, J.-M. Real Time TEM Imaging of Compression and Shear of Single Fullerene-Like MoS$_2$ Nanoparticle. *Tribol. Lett.* **2012**, *45*, 131–141. [CrossRef]

42. Tannous, J.; Dassenoy, F.; Lahouij, I.; Le Mogne, T.; Vacher, B.; Bruhács, A.; Tremel, W. Understanding the Tribochemical Mechanisms of IF-MoS$_2$ Nanoparticles Under Boundary Lubrication. *Tribol. Lett.* **2011**, *41*, 55–64. [CrossRef]

43. Xu, Y.; Hu, E.; Hu, K.; Xu, Y.; Hu, X. Formation of an adsorption film of MoS$_2$ nanoparticles and dioctyl sebacate on a steel surface for alleviating friction and wear. *Tribol. Int.* **2015**, *92*, 172–183. [CrossRef]

44. Dai, W.; Kheireddin, B.; Gao, H.; Liang, H. Roles of nanoparticles in oil lubrication. *Tribol. Int.* **2016**, *102*, 88–98. [CrossRef]

45. Hamrock, B.; Dowson, D. Minimum film thickness in elliptical contacts for different regimes of fluid-film lubrication. *Proc. Soc. Photo-Opt. Instrum. Eng.* **1978**.

46. Gonçalves, D.E.P.; Liñeira del Rio, J.M.; Comuñas, M.J.P.; Fernández, J.; Seabra, J.H.O. High Pressure Characterization of the Viscous and Volumetric Behavior of Three Transmission Oils. *Ind. Eng. Chem. Res.* **2019**, *58*, 1732–1742. [CrossRef]